# A Study on General State Model of Differential Drive Wheeled Mobile Robots

*Anh-Minh Duc TRAN*[1], *Tri-Vien VU* [2,*]

[1]Faculty of Electrical and Electronics Engineering, Ton Duc Thang University, Ho Chi Minh City, Vietnam
[2]Modeling Evolutionary Algorithms Simulation and Artificial Intelligence, Faculty of Electrical and Electronics Engineering, Ton Duc Thang University, Ho Chi Minh City, Vietnam

*Corresponding Author: Tri-Vien Vu (Email: vutrivien@tdtu.edu.vn)
(Received: 03-June-2023; accepted: 22-Agust-2023; published: 30-Sep-2023)
http://dx.doi.org/10.55579/jaec.202373.417

***Abstract.*** *This study introduces a novel approach by representing a multi-input-multi-output (MIMO) differential drive wheel mobile robot (DDWMR) using the standard state space representation for the first time. This representation facilitates the application of analysis and control system design techniques to MIMO systems. Specifically, the investigation delves into stability, controllability, observability, input-output interaction, and the relative gain array of the DDWMR model. To demonstrate the concept, the established methodology employs the conventional pole placement controller design technique to formulate a state feedback control law for trajectory tracking in the DDWMR system, utilizing both a nominal and a generalized model. The generalized model incorporates distinct parameters for the left and right motor-wheel systems, unlike the nominal model where they are assumed to be identical. Simulation results highlight that accounting for the asymmetric characteristics through the controller derived from the generalized model yields superior performance compared to the nominal model-based controller. Furthermore, the proposed model can be served as an illustrative platform for evaluating innovative MIMO control methodologies in prospective studies.*

***Keywords***

***Differential Drive, Wheel Mobile Robot, RGA, State Space, MIMO, Pole Placement.***

## 1. Introduction

Differential drive wheeled mobile robot is a robotic platform that uses independently controlled wheels on each side of its chassis to achieve movement and turning capabilities. Due to their mobility, DDWMRs can be used in a wide range of applications such as manufacturing and logistics, agriculture, search and rescue, military and defense, education and research [1–8]. This robot platform is considered highly nonlinear, non-holonomic constraint systems that make them a challenge for modeling and control [9]. To overcome the unmodelled dynamics, parameter uncertainty, and unknown disturbances, various nonlinear control techniques have been applied. In [10–12] authors used sliding mode control technique to handle the uncertainties and nonlinearities of wheeled mobile robots. In [13], the authors prosed an adaptive controller that can reject the effect of disturbances by fusing the robust and the sliding mode control techniques together. In [14], Roy *et. al.* solved the overestimation-underestimation problem of switching gain by using adaptive switching-gain-based robust con-

trol (ASRC). More recent evidence revealed that using a matrix-measure-based contraction approach, the intended guidance vector field's convergence to the task route was theoretically assured [15]. In [16], a nonlinear error feedback controller was utilized to track the outer loop intended velocities. In their works, Dogan *et. al.* studied the stability requirements of model reference adaptive control architectures with unstructured system uncertainties and unmodeled dynamics. They then synthesized adaptive and robust terms to ease the stability condition [17].

In DDWMRs, each side of the robot's chassis has its own independently driven wheel. This design typically consists of two wheels, one on the left side and one on the right side, where each wheel is actuated by its own electric motors that can be controlled separately in terms of speed and direction. The motors are interconnected and make DDWMRs coupling multi-input-multi-output systems. As a consequence, several MIMO control techniques have been applied for DDWMRs. In [18], authors used MIMO model predictive controller for autonomous trajectory tracking. In [19], the authors introduced a partially decentralized adaptive control approach for MIMO non-square systems. Recently, Rayguru *et al.* introduced a time-scale redesign-based saturation tracking controller for a class of feedback linearizable MIMO nonlinear systems [20].

Although many control systems for WMRs have been published, to the authors' knowledge, none of them have incorporated the full dynamics of the mechanical structure and actuators into a standard MIMO state space model. Furthermore, prior literature commonly presumed uniformity in the motor and wheel parameters in both sides of the robot chassis during modeling and control system design.

The aim of this study is to present a comprehensive model of a DDWMR in term of a general MIMO state-space representation. The parameters of the left and the right motor-wheel parts of the robot are not the same that make the model more practical and more generality. With the proposed MIMO state space model, modern techniques for analysis and control system design for MIMO systems can be applied for DDWMRs particularly as well as mobile robots in general. In additional, the proposed model can also be utilized as a benchmark model for evaluating novel MIMO control techniques beside well-known MIMO models such as continuously stirred tank reactor (CSTR) system.

The subsequent sections of this document are structured as follows. Section 2. provides a development of the mathematical model of the proposed DDWMR system. In section 3. , the proposed model is analyzed for stability, controllability, observability and interaction. The fourth section 4. outlines the design of the state feedback controller for the DDWMR system based on pole placement technique. Simulation results and discussion is presented in section 5. . Some conclusions are drawn in the final section.

# 2. Mathematical model

## 2.1. Differential Equations

The dynamic diagram of the proposed DDWMR is illustrated in $D$. In which $F_L$ and $F_R$ are traction forces at the ground contact points $C_L$ and $C_R$ of the driving wheels; $T_L$ and $T_R$ are the torque at the output shaft of the left and the right motor.

Assuming that the center of gravity (CoG) is at the intersection of the line linking the centers of the wheels, the robot's dynamic equations are

$$\begin{aligned} F_R + F_L &= m\frac{dV}{dt} \\ F_R - F_L &= \frac{J_z}{W}\frac{d\omega_z}{dt} \end{aligned} \tag{1}$$

where $m$ is the total weight of all the robot system, $J_z$ is the moment of inertia of the robot with respect to the z-axis, $V$ is the longitudinal velocity and $w_z$ is the angular velocity of the robot at the CoG.

Using the rolling without slipping assumption, the relationship between the robot velocities and the motor angular speed are given by

$$\begin{aligned} V &= \frac{R_{wR}}{2i_{gR}}\omega_R + \frac{R_{wL}}{2i_{gL}}\omega_L \\ \omega_z &= \frac{R_{wR}}{2Wi_{gR}}\omega_R - \frac{R_{wL}}{2Wi_{gL}}\omega_L \end{aligned} \tag{2}$$

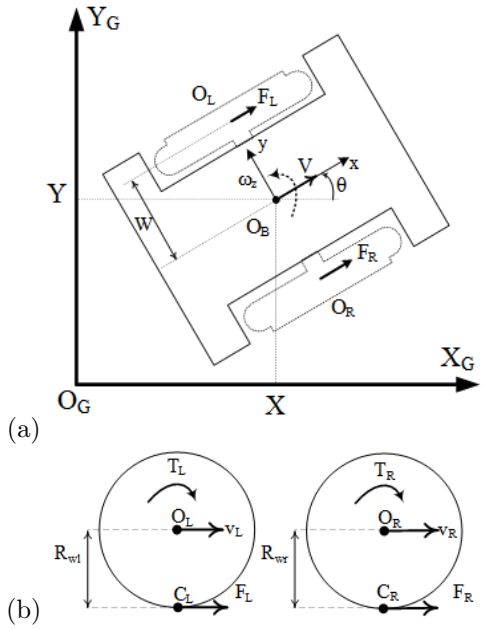


**Fig. 1:** Dynamic diagram of the system: (a) DDWMR and (b) the wheels.

where $2W$ is the distance from the right- to left-wheel's ground contact point, $R_{wR}$, $R_{wL}$ are the wheel radius; $\omega_R$ and $\omega_L$ are the angular speed of the right and the left wheel respectively.

The angular speeds of the motors are determined by the dynamic of the motor-wheel systems, given by:

$$\begin{aligned} J_{wR}\frac{d\omega_R}{dt} &= T_R - \frac{F_R}{i_{gR}\eta_{gR}}R_{wR} - B_{mR}\omega_R \\ J_{wL}\frac{d\omega_L}{dt} &= T_L - \frac{F_L}{i_{gL}\eta_{gL}}R_{wL} - B_{mL}\omega_L \end{aligned} \tag{3}$$

where $J_{wR}$, $J_{wL}$ are the moments of inertia of the wheel and motor, $B_{mR}$, $B_{mL}$ are the viscous coefficients of the motors, $i_{gR}$, $i_{gL}$ and $\eta_{gR}$, $\eta_{gL}$ are the gearbox ratio and efficiency of the right and the left motor, respectively.

The output torques of the PMDC motors are proportional to their armature currents as

$$\begin{aligned} T_R &= K_{tR}i_{aR} \\ T_L &= K_{tL}i_{aL} \end{aligned} \tag{4}$$

where $K_{tR}$ and $K_{tL}$ are the torque constant of the right and the left motor, respectively.

$$\begin{aligned} \frac{di_{aR}}{dt} &= -\frac{R_{aR}}{L_{aR}}i_{aR} - \frac{K_{tR}}{L_{aR}}\omega_R + \frac{1}{L_{aR}}V_{aR} \\ \frac{di_{aL}}{dt} &= -\frac{R_{aL}}{L_{aL}}i_{aL} - \frac{K_{tL}}{L_{aL}}\omega_L + \frac{1}{L_{aL}}V_{aL} \end{aligned} \tag{5}$$

where $R_{aR}$, $R_{aL}$ and $L_{aR}$, $L_{aL}$ are the resistance and inductance of the armature win-dings, $V_{aR}$ and $V_{aL}$ are the voltages applied to the armature winding of the motors.

Substitute Eq.(2) into Eq.(1) and solving for $F_R$ and $F_L$ we have

$$\begin{aligned} F_R &= \left(\frac{mR_{wR}}{4i_{gR}} + \frac{J_zR_{wR}}{4W^2i_{gR}}\right)\frac{d\omega_R}{dt} + \left(\frac{mR_{wL}}{4i_{gL}} - \frac{J_zR_{wL}}{4W^2i_{gL}}\right)\frac{d\omega_L}{dt} \\ F_L &= \left(\frac{mR_{wR}}{4i_{gR}} - \frac{J_zR_{wR}}{4W^2i_{gR}}\right)\frac{d\omega_R}{dt} + \left(\frac{mR_{wL}}{4i_{gL}} + \frac{J_zR_{wL}}{4W^2i_{gL}}\right)\frac{d\omega_L}{dt} \end{aligned} \tag{6}$$

Substitute Eq.(4) and Eq.(6) into Eq.(3) then we can obtain $\mathrm{d}\omega_R/\mathrm{dt}$ and $\mathrm{d}\omega_L/\mathrm{dt}$. Integrated with Eq.(5) the differential equations of the DDWMR can be expressed as

$$\begin{aligned} \frac{di_{aR}}{dt} &= k_{1R}i_{aR} + k_{2R}\omega_R + k_{3R}V_{aR} \\ \frac{d\omega_R}{dt} &= k_{4R}i_{aR} - k_{5R}\omega_R - k_{6R}i_{aL} + k_{7R}\omega_L \\ \frac{di_{aL}}{dt} &= k_{1L}i_{aL} + k_{2L}\omega_L + k_{3L}V_{aL} \\ \frac{d\omega_L}{dt} &= -k_{6L}i_{aR} + k_{7L}\omega_R + k_{4L}i_{aL} - k_{5L}\omega_L \end{aligned} \tag{7}$$

where

$$\begin{aligned} &k_{1R} = \tfrac{R_{aR}}{L_{aR}}, \quad k_{2R} = \tfrac{K_{tR}}{L_{aR}}, \quad k_{3R} = \tfrac{1}{L_{aR}} \\ &k_{4R} = \tfrac{C_L}{C_RC_L - C_{RL}C_{LR}}K_{tR}, \quad k_{5R} = \tfrac{C_L}{C_RC_L - C_{RL}C_{LR}}B_{mR} \\ &k_{6R} = \tfrac{C_{LR}}{C_RC_L - C_{RL}C_{LR}}K_{tL}, \quad k_{7R} = \tfrac{C_{LR}}{C_RC_L - C_{RL}C_{LR}}B_{mL} \\ &k_{1L} = \tfrac{R_{aL}}{L_{aL}}, \quad k_{2L} = \tfrac{K_{tL}}{L_{aL}}, \quad k_{3L} = \tfrac{1}{L_{aL}} \\ &k_{4L} = \tfrac{C_R}{C_RC_L - C_{RL}C_{LR}}K_{tL}, \quad k_{5L} = \tfrac{C_R}{C_RC_L - C_{RL}C_{LR}}B_{mL} \\ &k_{6L} = \tfrac{C_{RL}}{C_RC_L - C_{RL}C_{LR}}K_{tR}, \quad k_{7L} = \tfrac{C_{RL}}{C_RC_L - C_{RL}C_{LR}}B_{mR} \\ &C_R = J_{wR} + \tfrac{R_{wR}}{i_{gR}\eta_{gR}}\left(\tfrac{mR_{wR}}{4i_{gR}} + \tfrac{J_zR_{wR}}{4W^2i_{gR}}\right) \\ &C_{LR} = \tfrac{R_{wR}}{i_{gR}\eta_{gR}}\left(\tfrac{mR_{wL}}{4i_{gL}} - \tfrac{J_zR_{wL}}{4W^2i_{gL}}\right) \\ &C_L = J_{wL} + \tfrac{R_{wL}}{i_{gL}\eta_{gL}}\left(\tfrac{mR_{wL}}{4i_{gL}} + \tfrac{J_zR_{wL}}{4W^2i_{gL}}\right) \\ &C_{RL} = \tfrac{R_{wL}}{i_{gL}\eta_{gL}}\left(\tfrac{mR_{wR}}{4i_{gR}} - \tfrac{J_zR_{wR}}{4W^2i_{gR}}\right) \end{aligned}$$

Detail about modeling and simulation of each component can be found in our previous work [21].

### 2.2. State Space Representation

Let's $\mathbf{x} = \begin{bmatrix} i_{aR} & \omega_R & i_{aL} & \omega_L \end{bmatrix}^T$, $\mathbf{y} = \begin{bmatrix} V & \omega_z \end{bmatrix}^T$, $\mathbf{u} = \begin{bmatrix} V_{aR} & V_{aL} \end{bmatrix}^T$ are state, output, and input vectors, the general DDWMR model can be expressed in term of matrix as

$$\begin{aligned} \dot{\mathbf{x}} &= \mathbf{A}\mathbf{x} + \mathbf{B}\mathbf{u} \\ \mathbf{y} &= \mathbf{C}\mathbf{x} + \mathbf{D}\mathbf{u} \end{aligned} \tag{8}$$

where

$$\begin{aligned} \mathbf{A} &= \begin{bmatrix} -k_{1R} & -k_{2R} & 0 & 0 \\ k_{4R} & -k_{5R} & -k_{6R} & k_{7R} \\ 0 & 0 & -k_{1L} & -k_{2L} \\ -k_{6L} & k_{7L} & k_{4L} & -k_{5L} \end{bmatrix} \\ \mathbf{B} &= \begin{bmatrix} k_{3R} & 0 \\ 0 & 0 \\ 0 & k_{3L} \\ 0 & 0 \end{bmatrix} \\ \mathbf{C} &= \begin{bmatrix} 0 & k_{8R} & 0 & k_{8L} \\ 0 & k_{9R} & 0 & -k_{9L} \end{bmatrix} \\ \mathbf{D} &= \mathbf{O}_{2\times 2} \\ k_{8R} &= \frac{R_{wR}}{2i_{gR}}, \quad k_{9R} = \frac{R_{wR}}{2Wi_{gR}} \\ k_{8L} &= \frac{R_{wL}}{2i_{gL}}, \quad k_{9L} = \frac{R_{wL}}{2Wi_{gL}} \end{aligned} \tag{9}$$

It can be seen that the DDWMR is expressed in term of a standard multi-input-multi-output (MIMO) system. The system consists of two inputs: the voltages applied to the armature windings of the left and the right motor. The outputs are the linear and the angular speed of the robot while the states consist of the angular speed and the armature current of the motors. The interesting point is the parameters of the left and the right parts are not identical which is more generality.

## 3. Numerical analysis

To study the MIMO characteristic of the DDWMR, the system is first evaluated with numerical values listed in Table 1. Noticed that the parameters of the left and the right motor-wheel systems are not the same. The proposed model has more generality characteristic than all published works where the left and the right motor-wheel was typically assumed identical. The general DDWMR model in Eq.(8) with parameters in Table 1 had the following component matrices:

$$\begin{aligned} \mathbf{A} &= \begin{bmatrix} -43.04 & -36.54 & 0 & 0 \\ 76.83 & -1.609 & -14.22 & 0.2427 \\ 0 & 0 & -87.34 & -40.44 \\ -23.52 & 0.4926 & 31.1 & -0.5308 \end{bmatrix} \\ \mathbf{B} &= \begin{bmatrix} 57.97 & 0 \\ 0 & 0 \\ 0 & 78.43 \\ 0 & 0 \end{bmatrix} \\ \mathbf{C} &= \begin{bmatrix} 0 & 0.0169 & 0 & 0.0206 \\ 0 & 0.0844 & 0 & -0.1031 \end{bmatrix} \\ \mathbf{D} &= \mathbf{O}_{2\times 2} \end{aligned} \tag{10}$$

The MATLAB 'ss2tf' function could be used to determine the transfer function of the general DDWMR model in Eq.(10):

$$\begin{aligned} G_{V_{aR}V} &= \frac{V}{V_{aR}} = \frac{47s^2+4143s+84313}{s^4+133s^3+8104s^2+310485s+3226630} \\ G_{V_{aR}\omega_z} &= \frac{\omega_z}{V_{aR}} = \frac{516s^2+45276s+421564}{s^4+133s^3+8104s^2+310485s+3226630} \\ G_{V_{aL}V} &= \frac{V}{V_{aL}} = \frac{31s^2+1425s+124469}{s^4+133s^3+8104s^2+310485s+3226630} \\ G_{V_{aL}\omega_z} &= \frac{\omega_z}{V_{aL}} = \frac{-\left(346s^2+15226s+622344\right)}{s^4+133s^3+8104s^2+310485s+3226630} \end{aligned} \tag{11}$$

### 3.1. Pole and zero analysis

The poles of the general open-loop DDWMR system which also equal to the eigenvalues of the state space A matrix were $p_{1,2} = -23.302 \pm 49.947i$, $p_3 = -70.942$ and $p_4 = -14.973$. Fig. 2 showed the poles and zeros of the DDWMR transfer functions. All these poles were in the open left-half plane so the open-loop DDWMR system was stable. The natural frequencies were computed to be 14.973, 70.942 and 55,115 [rad/s], and the damping ratios were calculated to be 0.423 and 1.

### 3.2. Observability and controllability analysis

The controllability matrix of the general DDWMR system was calculated as [22]:

$$\begin{aligned} \mathbf{Co} &= \begin{bmatrix} \mathbf{B} & \mathbf{AB} & \mathbf{A^2B} & \mathbf{A^3B} \end{bmatrix} \\ \mathbf{Co} &= \begin{bmatrix} 58 & 0 & -2495 & 0 & -55359 & 40759 & 9660245 & -5401341 \\ 0 & 0 & 4454 & -1116 & -199191 & 99823 & -4702245 & -4187945 \\ 0 & 78 & 0 & -6850 & 55145 & 499648 & -7307696 & -34947774 \\ 0 & 0 & -1363 & 2440 & 61599 & -214915 & 2886441 & 14745622 \end{bmatrix} \end{aligned}$$

**Tab. 1:** Specifications of the general DDWMR model.

| Symbol | Description | Value | Units |
|---|---|---|---|
| $J_z$ | Moment of inertia of robot body | 0.35 | kg.m$^2$ |
| $m_b$ | Robot body mass | 15 | kg |
| $W$ | Half wheel base length | 0.2 | m |
| $m_{wR}$ | Right wheel mass | 2.55 | kg |
| $m_{wL}$ | Left wheel mass | 3.45 | kg |
| $J_{wR}$ | Right wheel inertia | 0.8e$^-$3 | Kg.m$^2$ |
| $J_{wL}$ | Left wheel inertia | 1.8e$^-$3 | Kg.m$^2$ |
| $i_{gR}$ | Right gearbox ratio | 2 | - |
| $i_{gL}$ | Left gearbox ratio | 2 | - |
| $\eta_{gR}$ | Right gearbox efficiency | 97.75 | % |
| $\eta_{gL}$ | Left gearbox efficiency | 72.25 | % |
| $R_{wR}$ | Right wheel radius | 0.0675 | m |
| $R_{wL}$ | Left wheel radius | 0.0825 | m |
| $B_{mR}$ | Right motor viscous coefficient | 0.0132 | N.m.s/rad |
| $B_{mL}$ | Left motor viscous coefficient | 0.0088 | N.m.s/rad |
| $K_{tR}$ | Right motor torque constant | 0.6303 | N.m/A |
| $K_{tL}$ | Left motor torque constant | 0.5157 | N.m/A |
| $L_{aR}$ | Right motor armature winding inductance | 0.0172 | H |
| $L_{aL}$ | Left motor armature winding inductance | 0.0127 | H |
| $R_{aR}$ | Right motor armature winding resistance | 0.7424 | Ω |
| $R_{aL}$ | Left motor armature winding resistance | 1.1136 | Ω |

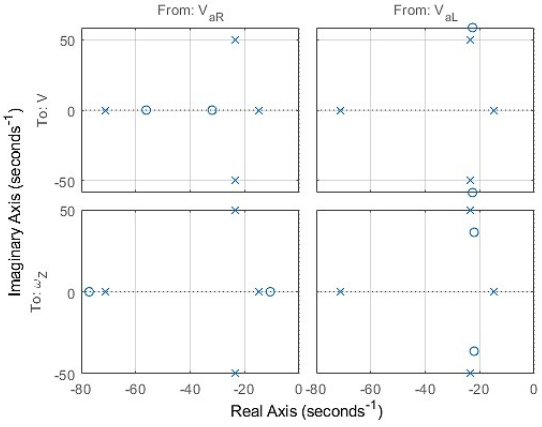


**Fig. 2:** Pole-Zero Map of the general DDWMR system.

The controllability matrix had full rank so the DDWMR system was controllable.

The observability matrix of the general DDWMR system was generated as [23]:

$$\mathbf{Ob} = \begin{bmatrix} \mathbf{C} & \mathbf{CA} & \mathbf{CA^2} & \mathbf{CA^3} \end{bmatrix}^T$$

$$\mathbf{Ob} = \begin{bmatrix} 0 & 0.017 & 0 & 0.021 \\ 0 & 0.084 & 0 & -0.103 \\ 0.811 & -0.017 & 0.401 & -0.007 \\ 8.908 & -0.187 & -4.408 & 0.075 \\ -36.1 & -29.6 & -35.0 & -16.2 \\ -399 & -325 & 390 & 178 \\ -342 & 1357 & 2977 & 1419 \\ -11979 & 15207 & -23894 & -15945 \end{bmatrix}$$

The rank of **Ob** was equal to the number of states so the system was observable.

## 3.3. Relative Gain Array (RGA)

Let G represent the transfer function of the general DDWMR system, from Eq. (11), we had

$$G = \begin{bmatrix} G_{V_{aR}V} & G_{V_{aL}V} \\ G_{V_{aR}\omega_z} & G_{V_{aL}\omega_z} \end{bmatrix} \tag{12}$$

The RGA of the non-singular square complex matrix G was a square complex matrix defined

as [22]

$$\mathrm{RGA}(G) = \Lambda(G) \triangleq G \times \left(G^{-1}\right)^{T} \tag{13}$$

For the $2\times2$ DDWMR transfer matrix, the RGA was

$$\mathrm{RGA}(G) = \begin{bmatrix} \lambda_{11} & \lambda_{12} \\ \lambda_{21} & \lambda_{22} \end{bmatrix} = \begin{bmatrix} \lambda_{11} & 1-\lambda_{11} \\ 1-\lambda_{11} & \lambda_{11} \end{bmatrix} \tag{14}$$

where

$$\lambda_{11} = \frac{1}{1 - \frac{G_{V_{aL}V} G_{V_{aR}\omega_z}}{G_{V_{aR}V} G_{V_{aL}\omega_z}}}$$

The RGA of a transfer matrix is generally computed as a function of frequency and provides a measure of interactions. Fig. 3 showed the frequency-dependent RGA for general DDWMR. At low and high frequency, $\Lambda(0) = \Lambda(j\infty) = \frac{1}{2}I$, there was a high degree of interaction [23] and it was impossible to control the $V$, and $\omega_z$ by only $V_{aR}$ or $V_{aL}$. At intermediate frequencies, the RGA off-diagonal elements were slightly greater than 0.5. For example, at frequency $\omega = 31.623$ rad/s, the RGA matrix became

$$\Lambda = \begin{bmatrix} 0.3355 + 0.0572\mathrm{i} & 0.6645 - 0.0572\mathrm{i} \\ 0.6645 - 0.0572\mathrm{i} & 0.3355 + 0.0572\mathrm{i} \end{bmatrix}$$

Nevertheless, the regulation of variables $V$ and $\omega_z$ solely through the manipulation of variables $V_{aR}$ or $V_{aL}$ remained unattainable Moreover,

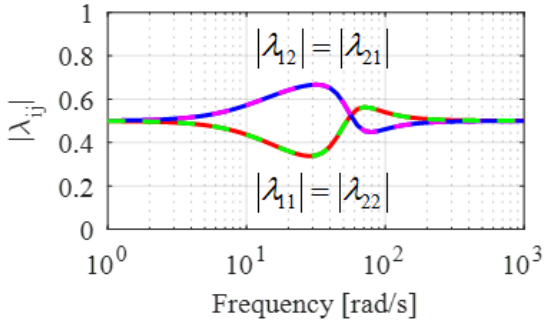


**Fig. 3:** Magnitude of RGA for general DDWMR.

when considering the angular velocity of the motors as outputs, the system could be represented in the form of transfer functions, as stated below:

$$\begin{aligned} \omega_R &= G_{RR}V_{aR} + G_{LR}V_{aL} \\ \omega_L &= G_{RL}V_{aR} + G_{LL}V_{aL} \end{aligned} \tag{15}$$

where the component transfer functions in the general model case are:

$$\begin{aligned} G_{RR} &= \frac{\Omega_R(s)}{V_{aR}(s)} = \frac{4454s^2+391056s+4996312}{s^4+133s^3+8104s^2+310485s+3226630} \\ G_{RL} &= \frac{\Omega_L(s)}{V_{aR}(s)} = \frac{-1363s^2-119088s}{s^4+133s^3+8104s^2+310485s+3226630} \\ G_{LR} &= \frac{\Omega_R(s)}{V_{aL}(s)} = \frac{-1116s^2-48012s}{s^4+133s^3+8104s^2+310485s+3226630} \\ G_{LL} &= \frac{\Omega_L(s)}{V_{aL}(s)} = \frac{2440s^2+108368s+6034851}{s^4+133s^3+8104s^2+310485s+3226630} \end{aligned} \tag{16}$$

Eq. (16) demonstrated that the speed of the right wheel is dependent not only on the voltage supplied to the right motor, but also the voltage supplied to the left motor, and vice versa. The interesting point is that, for a general DDWMR, the effect of the left armature voltage to the right angular speed is not the same as the effect of the right armature voltage to the left angular speed. This coupling phenomenon is a common problem in practice that makes controller design challenging.

## 4. Controller design

The location of the pole can be used to determine whether or not a system is stable. A stable system has a pole located to the left of the imaginary axis, whereas an unstable system has a pole located to the right of the imaginary axis. In order for the system to become stable, a control method is required to move the pole, which is to the right of the imaginary axis, to the left of the imaginary axis. Pole placement is a method of control that can position the pole appropriately. Conventional control techniques, such as pole placement, can also be used with MIMO systems, such as the DDWMR model used in this research. Using gain feedback, the system's desired design criteria can be met. The following is a diagram of the pole placement control system [21] In this method, the controlling law is:

$$\mathbf{u} = \mathbf{r} - \mathbf{K_C x} \tag{17}$$

In an effort to prevent steady-state errors caused by step references, this study adds two more integrators in series with the plant. The control framework is depicted in Fig. 5. We can model the addition of these integrators by augmenting our state equations with two extra states for the integral of the errors, which we will identify with

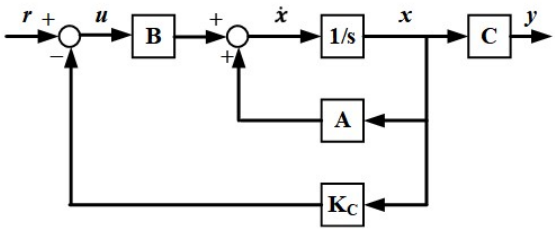


**Fig. 4:** Pole placement control system block diagram.

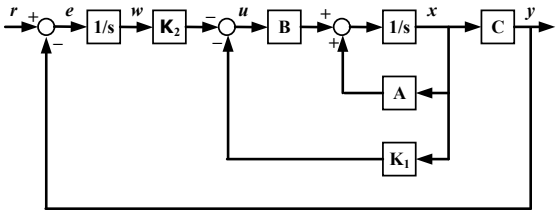


**Fig. 5:** Pole placement with integral control block diagram.

the variable $\mathbf{w}$ . This adds two extra state equations, where the derivative of these states are then just the errors $\mathbf{e} = \mathbf{w} = \mathbf{r} - \mathbf{y}$ . These equations will be placed at the bottom of our matrices. The reference $\mathbf{r}$ , therefore, now appears as additional inputs to our system. The output of the system remains the same.

$$\begin{aligned}\begin{bmatrix}\dot{\mathbf{x}}\\ \dot{\mathbf{w}}\end{bmatrix} &= \begin{bmatrix}\mathbf{A}_{4\times4} & \mathbf{0}_{4\times2}\\ -\mathbf{C}_{2\times4} & \mathbf{0}_{2\times2}\end{bmatrix}\begin{bmatrix}\mathbf{x}\\ \mathbf{w}\end{bmatrix}\\ &+\begin{bmatrix}\mathbf{B}_{4\times2}\\ \mathbf{0}_{2\times2}\end{bmatrix}\mathbf{u}+\begin{bmatrix}\mathbf{0}_{4\times2}\\ \mathbf{I}_{2\times2}\end{bmatrix}\mathbf{r},\\ \mathbf{y} &= \begin{bmatrix}\mathbf{C}_{2\times4} & \mathbf{0}_{2\times2}\end{bmatrix}\begin{bmatrix}\mathbf{x}\\ \mathbf{w}\end{bmatrix}.\end{aligned} \tag{18}$$

The control law is:

$$\mathbf{u} = -\mathbf{K}_1\mathbf{x} - \mathbf{K}_2\mathbf{w} \tag{19}$$

# 5. Simulation results and discussions

## 5.1. Open-loop step responses

In order to evaluate the performance of the proposed general DDWMR model, a nominal model of DDWMR (nominal DDWMR) is used. In the nominal DDWMR, the left- and the right-wheel-motor are identical. In this case the constants for the left and the rights become identical. The system matrices become:

$$\begin{aligned}\mathbf{A}_{nom} &= \begin{bmatrix}-61.87 & -38.2 & 0 & 0\\ 49.06 & -0.94 & -18.32 & 0.35\\ 0 & 0 & -61.87 & -38.2\\ -18.32 & 0.35 & 49.06 & -0.94\end{bmatrix},\\ \mathbf{B}_{nom} &= \begin{bmatrix}66.67 & 0\\ 0 & 0\\ 0 & 66.67\\ 0 & 0\end{bmatrix},\\ \mathbf{C}_{nom} &= \begin{bmatrix}0 & 0.01875 & 0 & 0.01875\\ 0 & 0.09375 & 0 & -0.09375\end{bmatrix},\\ \mathbf{D}_{nom} &= \mathbf{O}_{2\times2}.\end{aligned} \tag{20}$$

The transfer functions of the nominal DDWMR model were:

$$\begin{aligned}G_{V_{aR}V\_nom} &= \frac{V}{V_{aR}}\\ &= \frac{38s^2+2427s+101977}{s^4+126s^3+7809s^2+242215s+3213099}\\ G_{V_{aR}\omega_z\_nom} &= \frac{\omega_z}{V_{aR}}\\ &= \frac{421s^2+26301s+509887}{s^4+126s^3+7809s^2+242215s+3213099}\\ G_{V_{aL}V\_nom} &= \frac{V}{V_{aL}}\\ &= \frac{38s^2+2427s+101977}{s^4+126s^3+7809s^2+242215s+3213099}\\ G_{V_{aL}\omega_z\_nom} &= \frac{\omega_z}{V_{aL}}\\ &= \frac{-\left(421s^2+26301s+509887\right)}{s^4+126s^3+7809s^2+242215s+3213099}\end{aligned} \tag{21}$$

It can be seen that the effect of the left and the right armature voltages to the linear speed of the robot is the same while that effect to the angular speed is opposite. It is obvious because the right armature voltage causes the robot rotates counter clockwise while the left armature voltage causes the robot rotates clockwise.

The dissimilarity in the parameters of the motor and wheel components between the right and left sides of the general DDWMR resulted in distinct variations in the responses and quality metrics, including rise time, settling time, steady state, peak time, peak overshoot between the two sides of the general model in comparison to the nominal model. Fig. 6 illustrates the impact of the stochastic parameters in the general DDWMR model on the output of the system. Specifically, the general DDWMR model has distinct rise times and steady-state values for the output signals longitudinal velocity $V$ and yaw rate $\omega_z$ for the same input signal as a unit step voltage for two motors. The rise time of the $V$ response caused by $V_{aL}$ is three times that of

 

$V$ caused by $V_{aR}$ , and the steady state of $V$ caused by $V_{aL}$ is approximately 1.5 times that of $V$ caused by $V_{aR}$. Similarly, the rise time of the $\omega_z$ response induced by $V_{aL}$ is 7 times that of the $\omega_z$ response induced by $V_{aR}$, and the steady state of the $\omega_z$ response induced by $V_{aL}$ is nearly 1.5 times that of the $\omega_z$ response induced by $V_{aR}$. In addition, $\omega_z$'s response to $V_{aL}$ is a first-order system response, whereas $\omega_z$'s response to $V_{aR}$ is a second-order system response. The general model response's quality criteria are listed in Table 2.

## 5.2. Closed-loop step responses

With 1[m/s] longitudinal velocity $V$ and 1[radian/s] yaw rate $\omega_Z$ of the step references, the design criteria were the following:

- Settling time less than 0.1 seconds.
- Overshoot less than 2%.
- No steady-state error.

For the simulation of the system's response, the general DDWMR model was selected so that the effect of properly constructing the system's general model could be observed with clarity. In the simulation, two controllers were employed, one based on the nominal DDWMR model and the other on the general DDWMR model.

The Minimum ITAE Standard Forms [24] were utilized to calculate the desired characteristic polynomial of the system based on the aforementioned design specifications. $\omega_0$ was calculated to be 51.3 [rad/s] and was then replaced into the fourth order ITAE equation:

$$\Delta = s^4 + 2.41\omega_0 s^3 + 4.93\omega_0^2 s^2 + 5.14\omega_0^3 s + \omega_0^4 \tag{22}$$

The fourth order desired characteristics polynomial was

$$\Delta = s^4 + 124s^3 + 12975s^2 + 693993s + 6926639 \tag{23}$$

After obtaining the desired characteristic equation, the controller gain matrix that would generate the desired pole positions was determined using the MATLAB command 'place'.

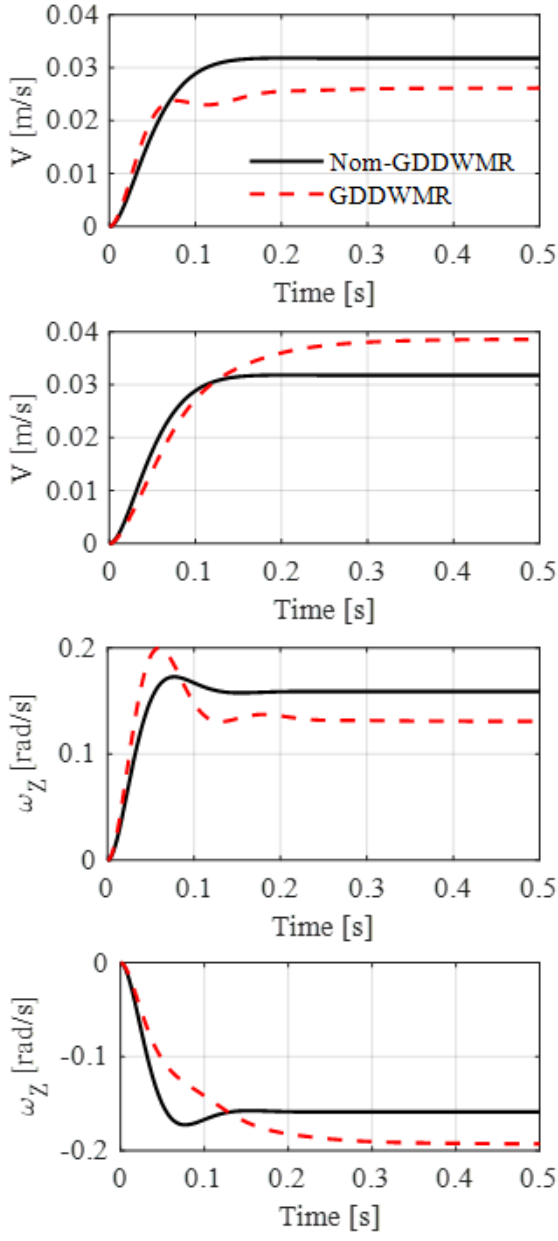


**Fig. 6:** Comparison of the open-loop step response of the nominal and general DDWMR $V_{aR}$, $V_{aL}$ to $V$, $\omega_z$.

The controller gain matrix calculated from the nominal DDWMR model was

$$\mathbf{K_C} = \begin{bmatrix} -0.1808 & 0.2933 & -0.7739 & -1.2434 \\ 0.8431 & 0.1258 & 0.1511 & 0.0579 \end{bmatrix} \tag{24}$$

**Tab. 2:** Transient qualities of general DDWMR.

| | From $V_{aR}$ to $V$ | $V_{aL}$ to $V$ | From $V_{aR}$ to $\omega_z$ | From $V_{aL}$ to $\omega_z$ |
|---|---|---|---|---|
| Rise time [s] | 0.057 | 0.153 | 0.021 | 0.148 |
| Settling time [s] | 0.219 | 0.28 | 0.223 | 0.27 |
| Steady state [m/s] | 0.0261 | 0.0386 | 0.131 | -0.193 |
| Peak time [s] | - | - | 0.059 | - |
| Peak overshoot [%] | 0 | 0 | 52.8 | 0 |

The remaining controller gain matrix calculated from the general DDWMR model was

$$\mathbf{K_C} = \begin{bmatrix} 0.2119 & 0.8089 & 0.7300 & 0.0126 \\ -0.2579 & -0.5592 & -0.2699 & -0.0318 \end{bmatrix} \tag{25}$$

The controller gain matrices presented above (PP controllers) were applied to the system diagram in Fig. 4. The closed-loop responses of longitudinal velocity and yaw rate to step references and right and left motor speed control signals were shown in Fig. 7. As demonstrated by the simulation results, the control signals emanating from the PP controllers were not congruent, the specified requirements were not met; specifically, the steady-state errors were excessively large.

In order to suppress the steady-state error in the system responses, the system diagram depicted in Fig. 5 was utilized. Apply the ITAE Minimum Standard Forms we obtained:

$$\Delta = s^6 + 3.93\omega_0 s^5 + 11.68\omega_0^2 s^4 + 18.56\omega_0^3 s^3 + 19.3\omega_0^4 s^2 + 8.06\omega_0^5 s + \omega_0^6 \tag{26}$$

the sixth order desired characteristic polynomial:

$$\Delta = s^6 + 202s^5 + 30740s^4 + 2505935s^3 + 133684131s^2 + 2864100332s + 18229880548 \tag{27}$$

and the relevant gain matrices for the controller calculated from the nominal DDWMR model were derived as follows:

$$\mathbf{K}_1 = \begin{bmatrix} 0.6033 & 1.8851 & -0.4502 & -0.4667 \\ 0.6346 & 1.9798 & 0.5367 & 3.3813 \end{bmatrix}$$
$$\mathbf{K}_2 = \begin{bmatrix} -298.55 & -200.61 \\ -2363.50 & 298.51 \end{bmatrix} \tag{28}$$

The remaining controller gain matrices calculated from the general DDWMR model were

$$\mathbf{K}_1 = \begin{bmatrix} 0.9169 & 1.4754 & -0.2594 & -1.2388 \\ 0.4541 & 1.2144 & 0.2032 & 3.6363 \end{bmatrix}$$
$$\mathbf{K}_2 = \begin{bmatrix} -273.05 & -367.16 \\ -1316.20 & 282.93 \end{bmatrix} \tag{29}$$

We simulated system responses by applying the controller in Eq. (28), (29) to the general model. The simulation outcomes were depicted in Fig. 8. The legend depicted in Fig. 8 comprised three distinct components. The initial section described the system model used for simulation, which was the general model. The following section elaborated on the controller derived from the nominal or general model. Lastly, the third segment represented the case-specific root mean square error (RMSE).

The findings indicated that the closed-loop responses of the system attained a steady state of zero without any overshooting. The settling time failed to satisfy the specified design criteria. In contrast to open-loop responses, the settling time had been significantly enhanced in closed-loop responses due to the considerably larger required steady-state value.

Furthermore, the results demonstrated that the response of the longitudinal velocity $V$ when utilizing the controller constructed from the nominal model has a faster reaction speed and a smaller RMSE than when employing the controller developed from the General model. However, when the yaw rate $\omega_z$ changes, the response of the longitudinal velocity $V$ when using the controller build from the nominal model is more affected. In contrast, the yaw rate $\omega_z$ response when using a controller designed from the general model has a slower reaction rate and a larger RMSE than when

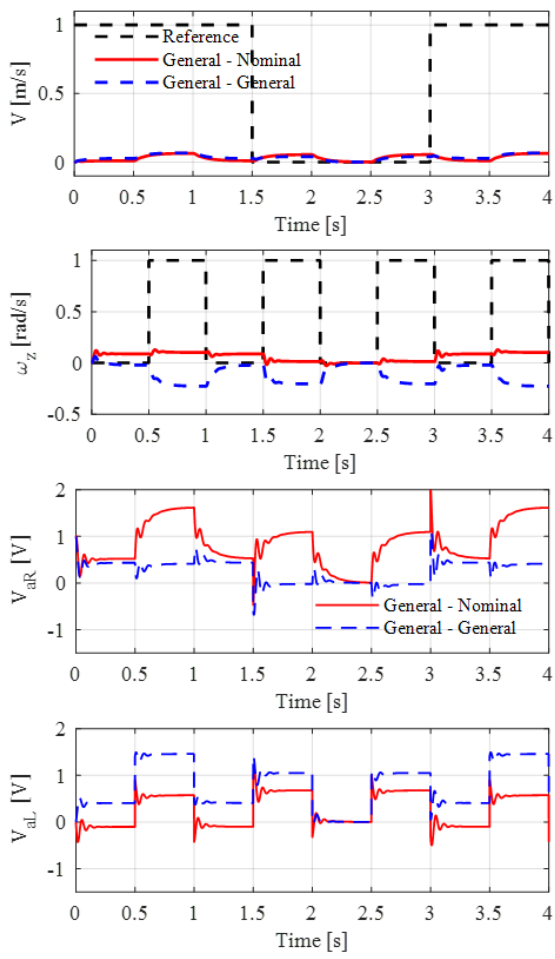


**Fig. 7:** Responses of the general DDWMR closed loop system with controllers designed by the pole placement method.

using a controller created from the nominal model. Changes in longitudinal velocity $V$ have a significant impact on the yaw rate $\omega_z$ response of a controller based on a nominal model. Simulation results indicated that the use of the controller developed from the general DDWMR model was superior to that of the controller created from the nominal DDWMR model.

# 6. Conclusion

This study presents the DDWMR in a standard MIMO system for the first time, assuming that the driving wheels roll without slipping. Two DDWMR models are proposed: a nominal version with identical left and right motor wheel systems and a more comprehensive general model allowing for different parameters. These models are carefully analyzed, evaluated, and simulated, demonstrating their versatility in allowing for the application of conventional or modern control methods. The study showcases the simplicity of controller design for the general asymmetric DDWMR system and demonstrates that the controller rooted in the general DDWMR model exhibits superior performance compared to its nominal counterpart. The proposed model has potential as a benchmark platform for evaluating the effectiveness of MIMO control techniques in future research and educational contexts. Overall, this study offers valuable insights into the development and application of DDWMR models in MIMO systems.

# References

[1] Rigelsford, J. (2004). Introduction to autonomous mobile robots. *Industrial Robot: An International Journal*, *31*, 534–535.

[2] Bekey, G. (2005). Autonomous robots: from biological inspiration to implementation and control. *MIT press*.

[3] Gao, X., Li, J., Fan, L., Zhou, Q., Yin, K., Wang, J., Song, C., Huang, L., & Wang, Z. (2018). Review of wheeled mobile robots' navigation problems and application prospects in agriculture. *IEEE Access*, *6*, 49248–49268.

[4] Bekey, G. & Yuh, J. (2008). The status of robotics. *IEEE Robotics & Automation Magazine*, *15*, 80–86.

[5] Nof, S. (1999). Handbook of industrial robotics. *John Wiley & Sons*.

[6] Calderon-Arce, C., Brenes-Torres, J.C., & Solis-Ortega, R. (2022). Swarm Robotics:

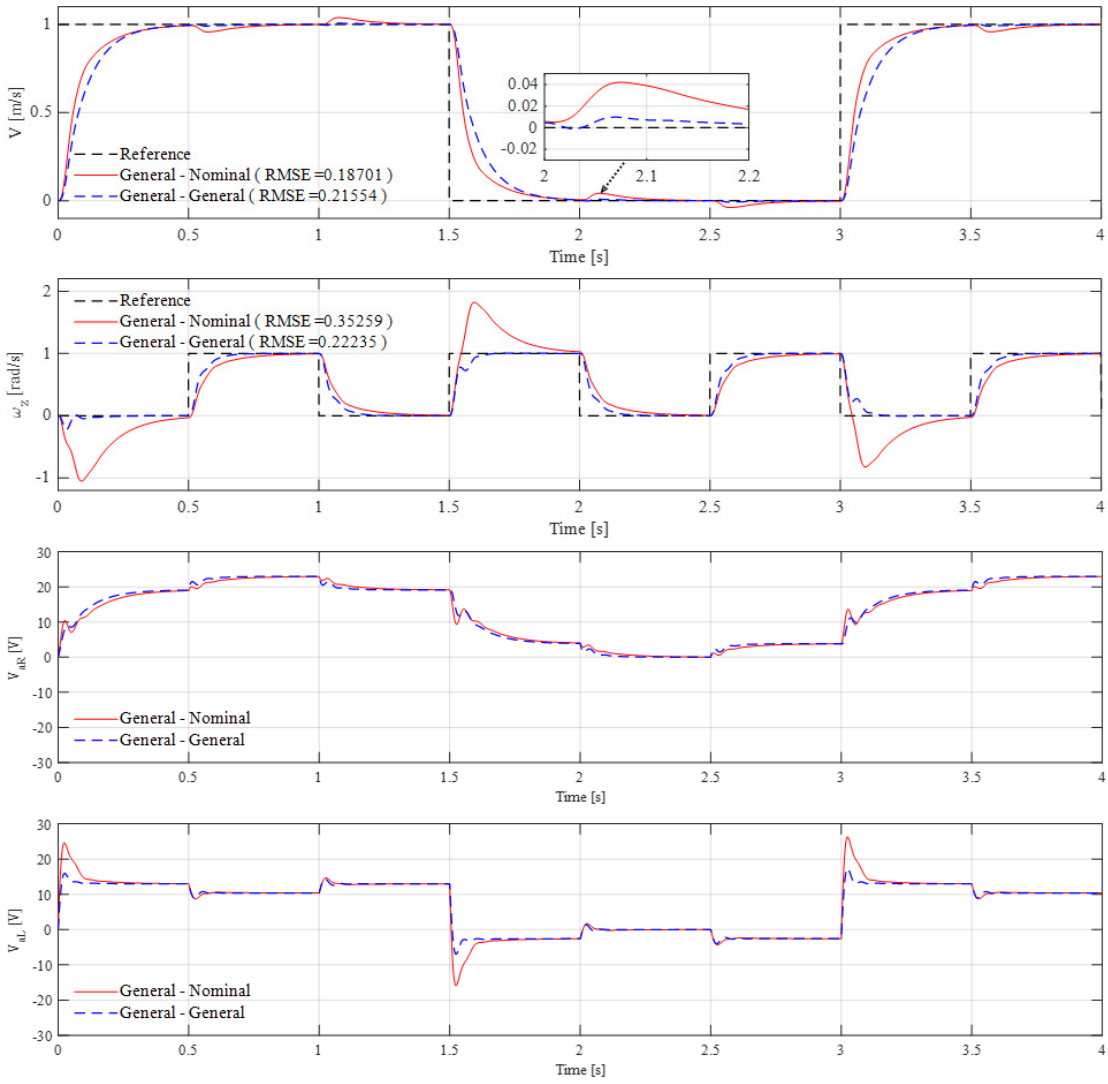


**Fig. 8:** Responses of the general DDWMR closed loop system with controllers designed by the pole placement method with integral control.

Simulators, Platforms and Applications Review. *Computation*, *10*, 80.

[7] Zelinsky, A. (2012). Field and service robotics. *Springer Science & Business Media*.

[8] Vu, T.V., Tran, A.M.D., Nguyen, B.H., & Tran, H.V.V. (2023). Development of Decentralized Speed Controllers for a Differential Drive Wheel Mobile Robot. *Journal of Advanced Engineering and Computation*, *7*, 76–94.

[9] Garcia-Sanchez, J.R., Silva-Ortigoza, R., Tavera-Mosqueda, S., Marquez-Sanchez, C., Hernandez-Guzman, V.M., Antonio-Cruz, M., Silva-Ortigoza, G., & Taud, H. (2017). Tracking control for mobile robots considering the dynamics of all their subsystems: Experimental implementation. *Complexity*, 5318504.

[10] Nguyen, T.B.T. (2017). Adaptive MIMO controller design for chaos synchronization in coupled josephson junctions via fuzzy neural networks. *Journal of Advanced En-*

 

*gineering and Computation*, *1*, 80–86.

[11] Lai, B.H., Tran, A.T., Pham, N.T., & Huynh, V.V. (2021). Sliding mode load frequency regulator for different-area power systems with communication delays. *Journal of Advanced Engineering and Computation*, *5*, 93–107.

[12] Nguyen, T.C., Hien, C.T., & Phan, D.V. (2022). Single Phase Second Order Sliding Mode Controller for Mismatched Uncertain Systems with Extended Disturbances and Unknown Time-Varying Delays. *Journal of Advanced Engineering and Computation*, *6*, 122–135.

[13] Naderi, M. & Fard, J.T. (2017). Adaptive control of the wheeled mobile robots' dynamic model with regard to the limitation of input torques. *QUID: Investigacion, Ciencia y Tecnologia*, 1167–1174.

[14] Roy, S., Roy, S.B., & Kar, I.N. (2017). Adaptive–robust control of Euler–Lagrange systems with linearly parametrizable uncertainty bound. *IEEE Transactions on Control Systems Technology*, *26*, 1842–1850.

[15] Chen, J., Wu, C., Yu, G., Narang, D., & Wang, Y. (2021). Path following of wheeled mobile robots using online-optimization-based guidance vector field. *IEEE/ASME Transactions on Mechatronics*, *26*, 1737–1744.

[16] Li, P., Yang, H., Li, H., & Liang, S. (2022). Nonlinear ESO-based tracking control for warehouse mobile robots with detachable loads. *Robotics and Autonomous Systems*, *149*, 103965.

[17] Dogan, K.M., Yucelen, T., & Muse, J.A. (2022). Adaptive control systems with unstructured uncertainty and unmodelled dynamics: a relaxed stability condition. *International Journal of Control*, *95*, 2211–2224.

[18] Malouche, I. & Bouani, F. (2017). Realtime Application of Constrained Predictive Control for Mobile Robot Navigation. *International Journal of Advanced Computer Science and Applications*, *8*.

[19] Malouche, I. & Bouani, F. (2018). A new adaptive partially decentralized PID controller for non-square discrete-time linear parameter varying systems. *International Journal of Control, Automation and Systems*, *16*, 1670–1680.

[20] Rayguru, M.M., Roy, S., & Kar, I.N. (2019). Time-scale redesign-based saturated controller synthesis for a class of MIMO nonlinear systems. *IEEE Transactions on Systems, Man, and Cybernetics: Systems*, *51*, 4681–4692.

[21] Dorf, R.C. & Bishop, R.H. (2011). Modern control systems. *Pearson*.

[22] Bristol, E. (1966). On a new measure of interaction for multivariable process control. *IEEE transactions on automatic control*, *11*, 133–134.

[23] Magaji, N. & Mustafa, M.W. (2010). Relative gain array Interaction Analysis of UPFC Device for damping Oscillations. *System*, *6*, 7.

[24] Graham, D. & Lathrop, R.C. (1953). The synthesis of "optimum" transient response: criteria and standard forms. *Transactions of the American Institute of Electrical Engineers, Part II: Applications and Industry*, *72*, 273–288.

## About Authors

**Tri-Vien VU** received the B.Eng. degree in mechatronics from Hanoi University of Science and Technology Ha Noi, Vietnam, in 2005, and the M.Sc. and Ph.D. degrees from Da-yeh University, Changhua, Taiwan in 2011 and 2015, respectively, all in mechanical and automation engineering. He joined the Faculty Electrical and Electronics Engineering, Ton Duc Thang University, Ho Chi Minh City, Vietnam, and work as a Lecturer since 2015. His research interests include vehicle dynamic, mobile robot, power electronics, electrical drives.

**Anh Minh D. TRAN** got his B.S. and M.S. degrees in Control and Automation Engineering from Ho Chi Minh City University of Transport in 2008 and Ho Chi Minh University of Technology in 2013, respectively, and his Ph.D. from Pukyong National University in Busan, Korea, in 2017. He is currently a lecturer at the Faculty of Electrical and Electronics Engineering at Ton Duc Thang University in Ho Chi Minh City, Vietnam. His scientific interests include control theory, computer vision, vehicle dynamics, and mobile robots with applications to industry and the environment. He can be contacted by email at: tranducanhminh@tdtu.edu.vn.